Proc. NIPR Symp. Antarct. Meteorites, **9**, 218–236, 1996

FORMATION PROCESSES OF MAGNETIC SPHERULES COLLECTED FROM DEEP-SEA SEDIMENTS —OBSERVATIONS AND NUMERICAL SIMULATIONS OF THE ORBITAL EVOLUTION—

Toru YADA, Tomoki NAKAMURA, Minoru SEKIYA and Nobuo TAKAOKA

Department of Earth and Planetary Sciences, Faculty of Science, Kyushu University 33, Hakozaki, Fukuoka 812–81

Abstract: Spherules collected from deep-sea sediments were analyzed for major chemical compositions and examined for textural relationships. Two main types of internal texture are observed in Ni-bearing I-type spherules: spherules with Ni-free Fe-oxide mantle and Fe-Ni metallic cores and Fe-Ni oxide spherules without metallic cores. Cores are often observed off-centered. S-type spherules show porphyritic, barred, and fine-grained types of texture. Relict olivine grains are found in some porphyritic S-type spherules. A cooling rate of 55°C/s was calculated for one of these grains based on chemical zonal patterns. For I-type spherules, numerical simulations were performed to constrain the relationship between temperatures, radii of spherules, and the apparent gravitational acceleration with the spherule as a stationary frame of reference. Results indicate that a) spherules lose most of their original mass by evaporation over 1900°C, and, b) the apparent gravitational acceleration is at a maximum during the last stage of evaporation. Based on the observations and numerical simulations of I-type spherules, we propose the following model for their formation: during ablation, the metallic core is off-centered, a surface of the core is then exposed to the air due to the strong apparent gravitational acceleration and, finally, oxidation reactions can proceed on the exposed core surface.

1. Introduction

Spherules in deep-sea sediments have long been studied since 1883 (MURRAY and RENARD, 1883). We now know that these spherules originated in an extraterrestrial environment because many contain wüstite (MARVIN and EINAUDI, 1967), the enrichments of Ni, Co (SMALES *et al.*, 1958) and Ir (MILLARD and FINKELMAN, 1970) and/or the presence of cosmogenic nuclides, such as ^{53}Mn (NISHIIZUMI, 1983), ^{26}Al and ^{10}Be (RAISBECK *et al.*, 1986).

Spherules are grouped into iron (I), stony (S) and glassy (G) types based on chemical and/or mineral compositions (*e.g.*, BLANCHARD *et al.*, 1980; BROWNLEE, 1985). I-type spherules are subdivided into Fe-Ni spherules and Fe spherules without Ni, which are more common. S-type spherules consist mainly of olivine, magnetite and glass. Sometimes they contain relict grains, such as forsterite, enstatite and other minerals. G-type spherules consist of transparent glass and are relatively rare compared to the other types of spherules.

Of the three types of spherules, the formation processes of I-type spherules may be the easiest to deduce because only these contain essentially three elements, Fe, Ni and

O. The oxidation of I-type spherules probably occurred in the terrestrial environment since the oxygen isotopes of I-type spherules plot on the terrestrial fractionation line (CLAYTON *et al.*, 1986). Therefore, most of the oxygen atoms in I-type spherules are probably terrestrial. By analogy with the metal compositions in meteorites, the precursor of I-type spherules may be a Fe-metal containing 5 to 10% Ni. The oxidation of Fe-metal in spherules probably occurred during melting at atmospheric entry.

A clearer picture of the origin of I-type spherules is beginning to emerge. For example, BROWNLEE *et al.* (1984) argue convincingly that interplanetary dust particles are melted by heating during atmospheric entry to form silicate melt and metallic melt. Individual spherules are then separated into a silicate melt sphere and a metallic one due to density difference. Iron in metallic sphere oxidized leaving a high Ni metallic core. Oxidation persisted and the Ni-rich core is also oxidized. Finally, residues in the core formed a Pt group nugget. This scenario is consistent with the resistivity against oxidation, which increases in the order of Fe, Ni and Pt group elements. BI *et al.* (1993) reported that a Ni-rich metallic core escaped from Ni-free Fe-oxide mantle to form a Ni-Fe metallic spherule whose Ni content ranges from 27 to 100%. The left mantle forms a Fe-oxide spherule without Ni.

Although significant progress has been made in our understanding the formation processes of I-type spherules, the conditions of spherule formation have never been estimated quantitatively. In this paper, we characterize the structure and chemistry of I-type spherules, and use this data in a numerical simulation to constrain the conditions and formation processes of I-type spherules.

2. Samples and Analytical Techniques

Spherules were separated from deep-sea sediments that were dredged up from 5800 m in depth offshore Hawaiian Islands (9°30'N, 174°17'W). The surface texture and chemical composition of each spherule was analyzed using an EPMA (JEOL JCXA733, emission current: 1×10^{-8} A and accelerating voltage: 20 kV in metal mode; same current and 15 kV accelerating voltage in silicate mode). The surface texture of the spherules was observed first, then polished sections were made to observe their internal texture. The EPMA surface observation shows that seventy-five spherules ranging in size from 20 to 300 μm are identified as I-type and forty-one spherules ranging size from 70–230 μm as S-type.

3. Petrology

3.1. S-type spherules

The surface texture of S-type spherules can be separated into porphyritic type (Fig. 1a), barred type (Fig. 1b) and fine-grained type (Fig. 1c). Differences in the surface texture are carried through into the internal structure, as shown in Figs. 1d, e and f. S-type spherules consist mainly of olivine and magnetite. Porphyritic and fine-grained types sometimes have relict olivine grains which provide useful information about precursor materials. Relict olivine grains have almost pure forsteritic compositions ($\leq Fa_5$), and Fe-Ni metal inclusions (Fig. 1g). If, instead, these relict forsterite grain had melted,

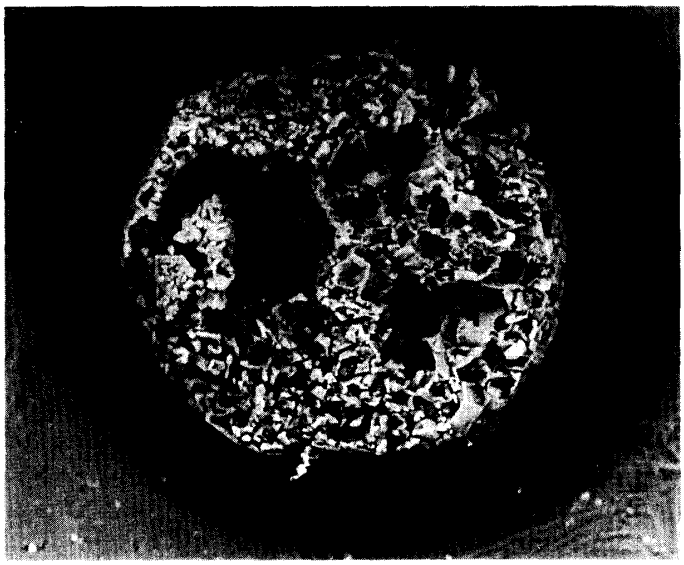

Fig. 1. Backscattered-electron images of S-type spherules. (a), (b) and (c) show surface morphologies, and (d), (e) and (f) show internal textures of (a), (b) and (c) spherules, respectively.

Fig. 1a. Porphyritic S-type spherule SS-1 with approximately 120 μm in diameter and contains of olivine grains. Surface grains of the spherule appear black due to alteration reactions on the sea floor.

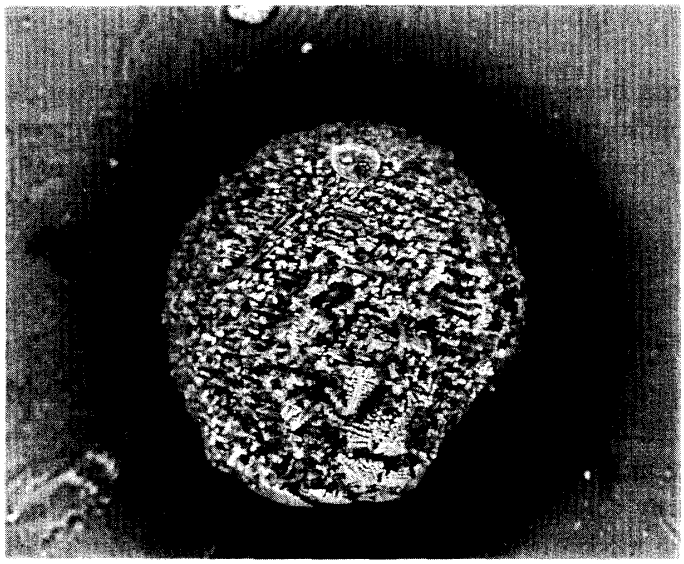

Fig. 1b. Barred S-type spherule SS-2 with 190 μm in diameter. Dendritic magnetites grow on the surface of barred olivine.

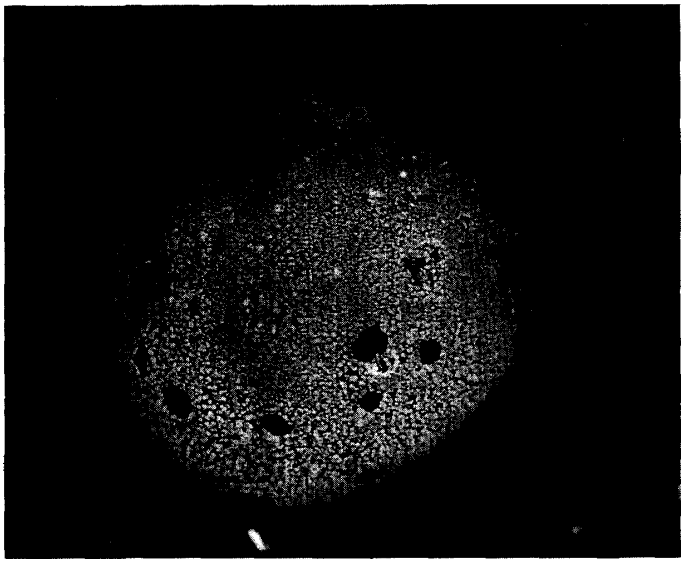

Fig. 1c. Fine-grained S-type spherule SS-3 that is 170 μm in diameter contains fine olivine grains, each to which are around 1 μm in size. Several voids are present on the spherule.

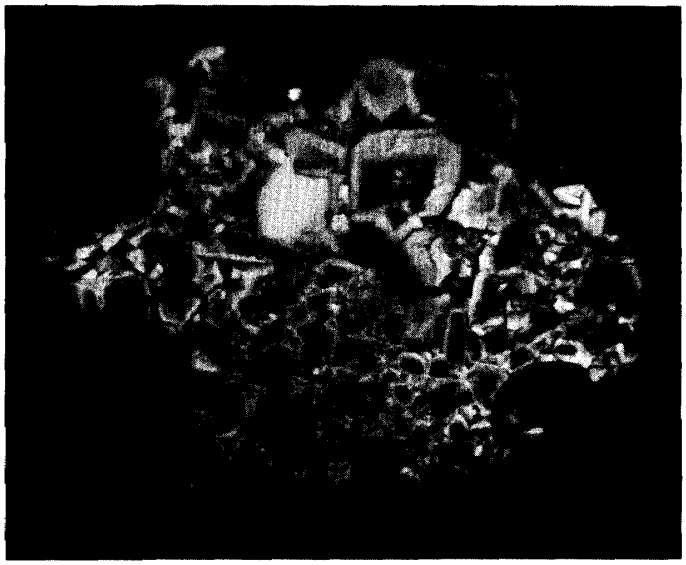

Fig. 1d. Olivine grains are over 10 μm in size in the cross section of SS-1. The inner parts of most grains have become hollow probably due to alteration on the sea floor (dark area surrounded by right rim). Vertical width of the spherule is 90 μm.

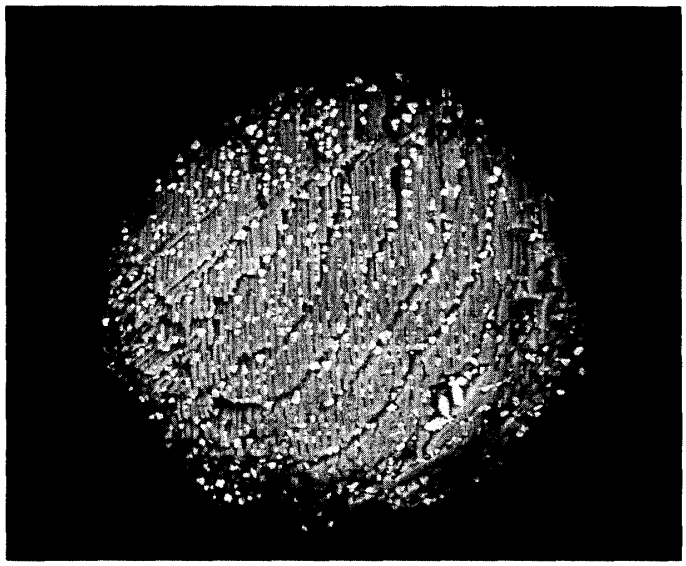

Fig. 1e. Barred olivine around 2 μm in width and fine grained magnetite (bright ones) are observed in internal texture of SS-2. Vertical width of the spherule is 155 μm.

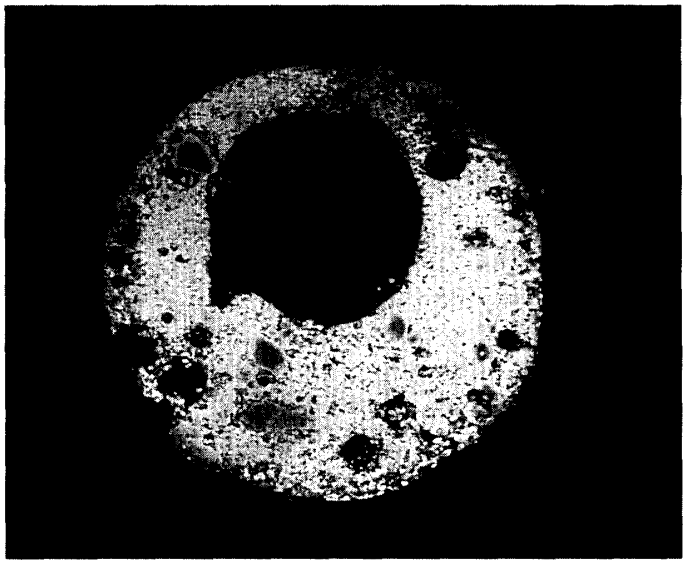

Fig. 1f. Internal texture of SS-3 consists of very fine grains of olivine and magnetite, and large Fe-poor olivine grains. Some vesicles are observed; the largest one is 80 μm across. Vertical width of the spherule is approximately 170 μm.

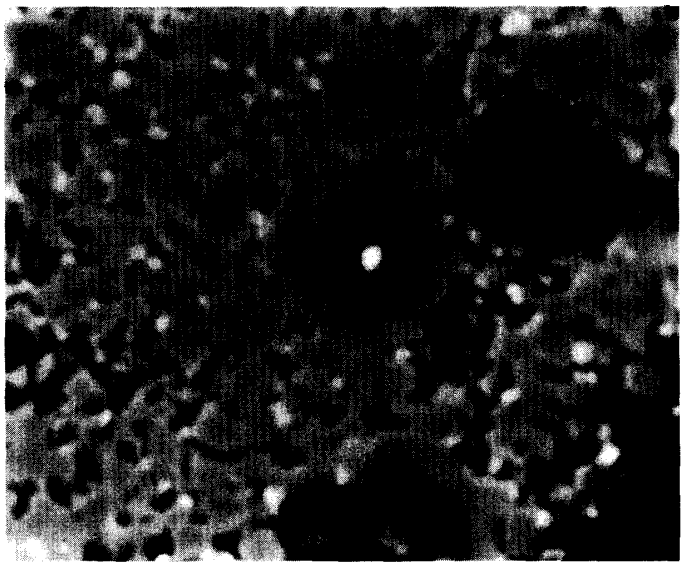

Fig. 1g. An enlarged image of lower right part of SS-3. The olivine grain located in the center of photograph exhibits chemical zonation. The FeO concentration increases from core to rim. Kamacite is present in the olivine grain (bright grain in the center). This disequilibrium state indicates that the olivine grain is relict.

Fig. 2a. The spherule SS-4 is 125 μm in diameter and contains about 30 relict forsterite grains with zonal structure. The wight matrix surrounding the relict grains has composition of (Fe, Ni)$_{12}S_{13}$.

Fe-Ni metal would have either been oxidized to become magnetite or dispersed into the olivine as FeO.

Relict olivine grains often preserve a zonal structure that probably formed with heating during atmospheric entry (Fig. 2a), as reported by BLANCHARD *et al.* (1980). The Fa content of olivine increases gradually from $\leq Fa_5$ to $\geq Fa_{40}$ from the centers to the edges of the grains. During heating, then, Fe^{2+} ions must have diffused into forsterite from the edge to the center by exchanging Mg^{2+}. Distributions of Fa can be calculated on the basis of diffusion coefficients of Fe^{2+} in forsterite with various cooling rates from peak temperatures. By comparing with the Fa distribution calculated with the measured one, the cooling rates for the olivine grains can be estimated (MIYAMOTO *et al.*, 1986). Cooling rates were assumed to be constant and profiles were calculated for cooling rates that ranged from 1.2×10^{-3} to 83°C/s with peak temperatures ranging from 1000 to 1800 °C. Some of the calculated Fa distributions and the observed one (an arrow in Fig. 2a)

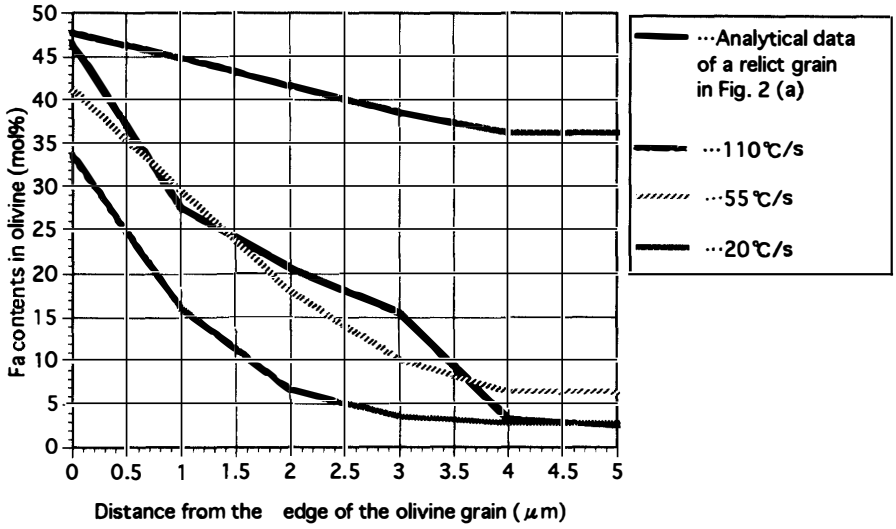

Fig. 2b. Cooling rates of a relict grain in SS-4 (arrow) calculated with peak temperature of 1700°C. 55°C/s is obtained for the cooling rate of the grain by profile fitting with calculated and the analytical data.

are shown in Fig. 2b. These results indicate that the zonation in the relict olivine grain is best explained by a cooling rate of 55°C/s and a peak temperature of 1700°C.

3.2. I-type spherules

The surface texture of I-type spherules can be separated into dendritic type (Fig. 3a), polygonal type (Fig. 3b) and smooth type (Fig. 3c). Many of these contain craters, dents and/or flat or concentric-scale structures (on the center of spherule in Fig. 3b and the right side of spherule in Fig. 3c) were observed. After the surface observation, twenty-seven I-type spherules were polished and analyzed for the internal chemical composition. The chemical compositions of all analyzed points in Fig. 3d–f are shown in Table 1. The spherules containing Ni were preferentially selected for polishing, and approximately 40% of these spherules had Ni/Fe ratios above 0.05, equal to the cosmic ratio. Two types of internal texture are observed in the Fe-Ni spherules. The first type is composed of a Ni-free Fe-oxide spherule with a Fe-Ni metallic core (Fig. 3d). The second one is of a Fe-Ni oxide spherule (Fig. 3e) with no core. Many of these contain exsolution structures, and one exceptional example contains a large round hole (Fig. 3f). Previous workers reported Fe-Ni oxide spherules with Ni-rich cores (BLANCHARD *et al.*, 1980; BROWNLEE, 1985), but it is likely that reactions with sea water served to disperse NiO from the original core into the surrounding mantle. The hole is possibly a mold of a metallic core which was somehow lost, because Ni enrichment around the hole (Table 1) suggests the existence of a Ni-rich core. However, it is not clear that whether the heterogeneity of the Ni concentration occurred during atmospheric ablation or sea floor processes. Most of metallic cores are off-centered in spherules, suggesting the influence of a very large physical force.

Our chemical analyses indicate that the Ni and Co in Fe-Ni spherules concentrate within metallic cores. Figure 4 shows a plot of the Co concentration against Ni for Fe-Ni metallic cores, together with data by CZAJKOWSKI (1987). The Ni concentration in-

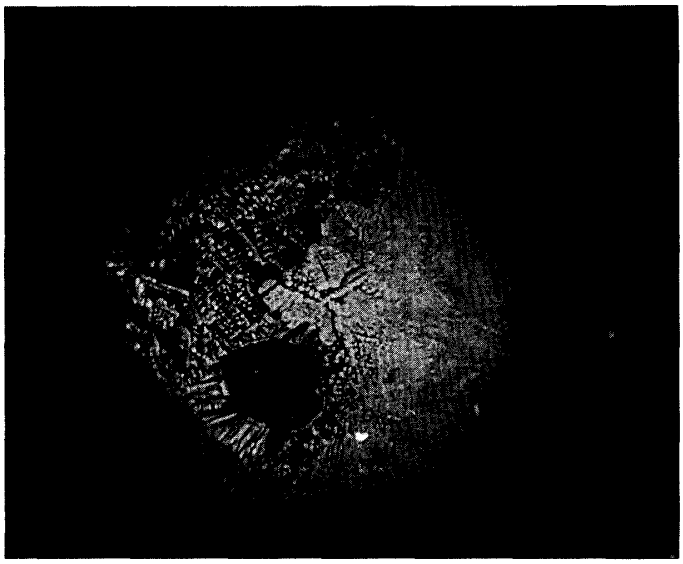

Fig. 3. Backscattered electron images of I-type spherules. (a), (b) and (c) give typical surface textures of I-type spherules. (d), (e) and (f) show cross sections of I-type spherules containing Ni. Numbered arrows shows locations analyzed with EPMA. The results are given in Table 1.

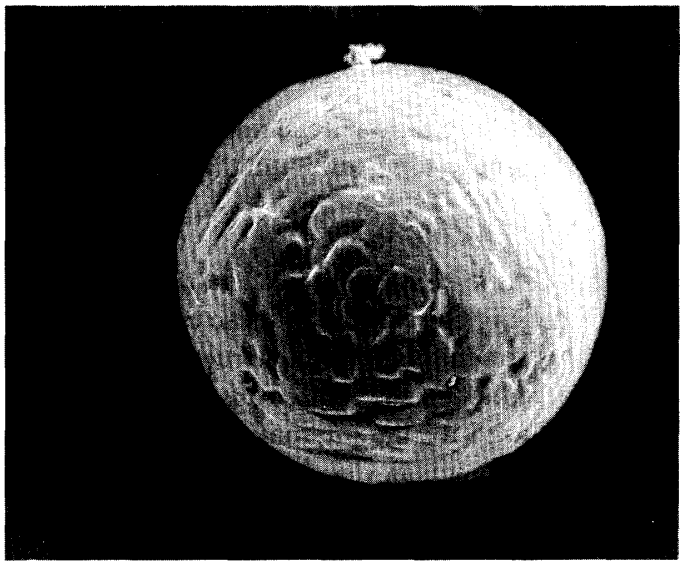

Fig. 3a. Dendritic I-type spherule IS-1 with 100 μm in diameter, and composed of dendritic magnetite. A round crater is present on the surface. This type of spherules contains dendritic structure of variable widths.

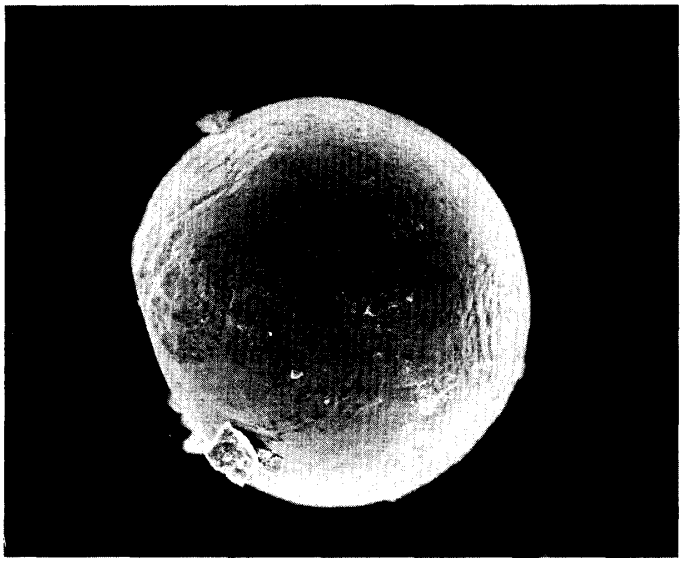

Fig. 3b. Polygonal I-type spherule IS-2 consisting of Fe-Ni oxide with 110 μm in diameter. Many polygonal shapes can be observed on its surface.

Fig. 3c. Smooth I-type spherule IS-3 has a diameter of 200 μm. The surface is smooth with few wrinkles and has a flat part on lower left side.

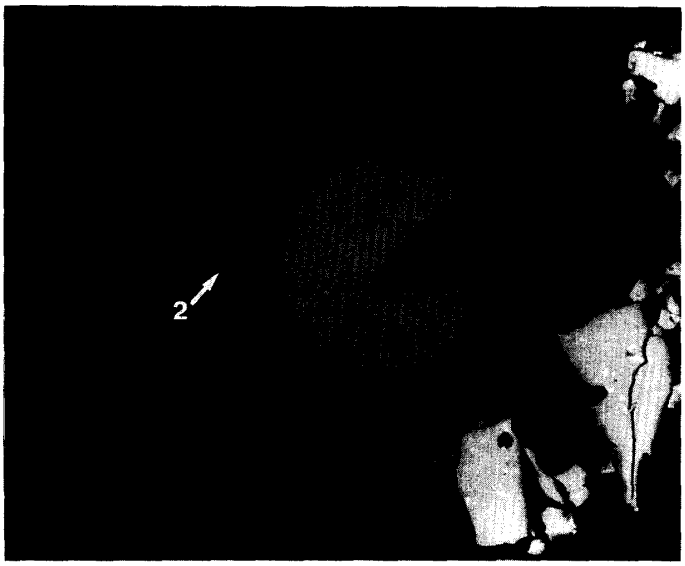

Fig. 3d. Spherule IS-4 is approximately 90 μm in diameter, and Ni-free with a Fe oxide mantle and a Fe-Ni metallic core. The dark grey outer layer is magnetite and the bright off-centered core is taenite with a Ni content of 39 wt% (Table 1).

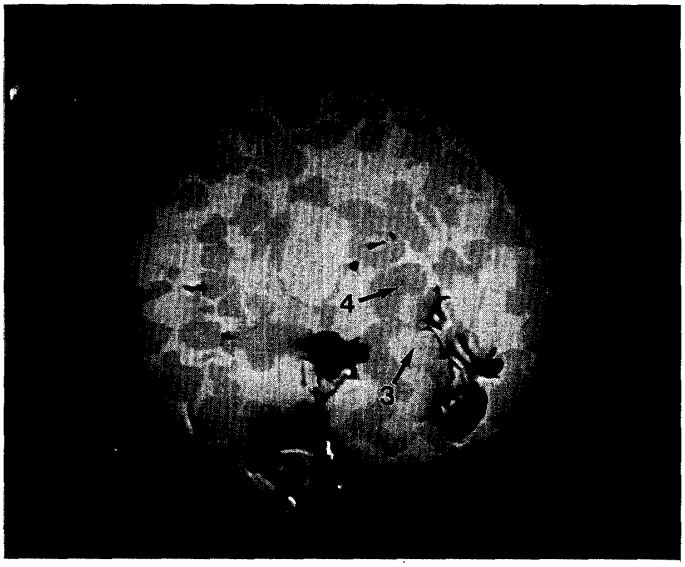

Fig. 3e. Fe-Ni oxide spherule without a core IS-3 is approximately 100 μm in diameter. An exsolution structure is observed, where brighter area is richer in Ni content than the dark area.

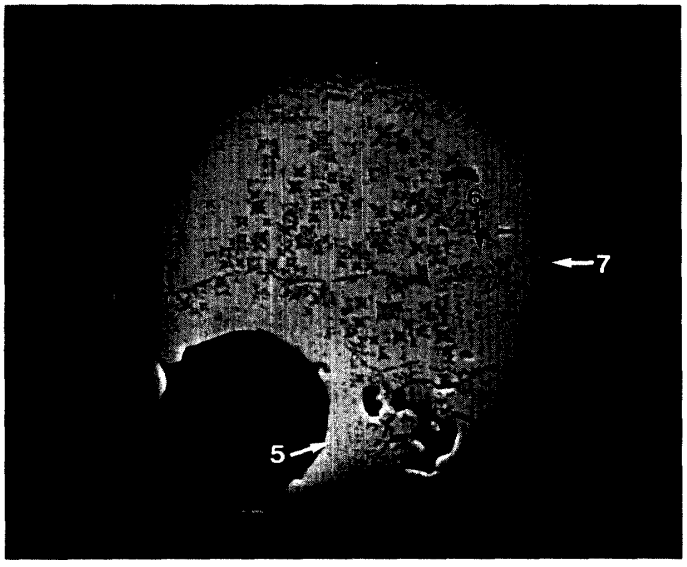

Fig. 3f. Fe-Ni oxide spherule IS-5 is 90 μm in diameter with a round mold. The mold in lower left part of the spherule presumably formed by the expulsion of core after the spherule had solidified. The mantle exhibits an exsolution structure and the Ni is richest in the brightest portions of the structure.

Table 1. Chemical compositions of the interior of I-type spherules. Numbers of analytical points are given in Figs. 3d, e, and f.

Sample No.	IS-4		IS-3		IS-5		
Analytical point	1	2	3	4	5	6	7
Ni	39.49	0.18	5.07	3.15	20.14	14.5	10.03
Fe	59.72	71.99	68.07	65.79	50.8	56.99	56.2
S	0.02	0.01	0.01	0.01	0.01	n. d.	n. d.
Co	2.13	0.07	0.46	0.23	0.96	0.85	0.57
Cr	n. d. [a]	0.20	0.01	0.02	0.03	0.01	0.03
Total (wt%)[b]	101.36	72.46	73.63	69.21	71.94	72.35	66.83

[a] n. d. =not detected.

[b] wt% values less than 100 due to excess oxygen.

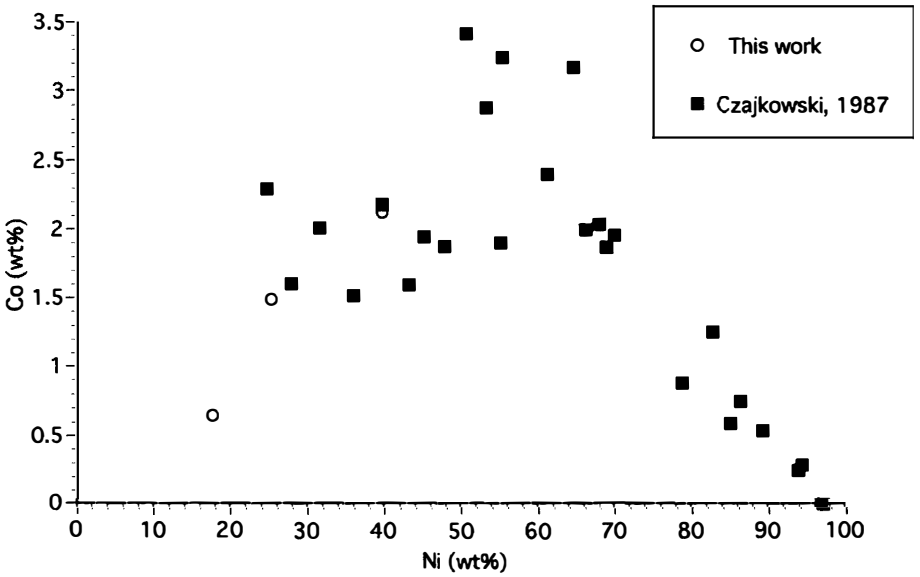

Fig. 4. Correlation between Co and Ni concentrations. Between 0 and 50 wt% Ni, Co has positive correlation with Ni, while negative correlation with Ni between 50 and 100 wt% Ni, suggesting that oxidation of Co begins when Ni reaches around 50 wt% in the core.

creases with decreasing Fe. In the range of 0–50 wt% Ni, Co shows a positive correlation with Ni. However, in the range of 50–100 wt% Ni, Co shows a negative correlation. In this case, the oxidation of Fe in a metallic core produces commensurate increase of Ni and Co. Thus, Co is not oxidized when Fe content is greater than Ni, but it does become oxidized after most of Fe has been oxidized. Again, this is probably due to the tendency for oxidation to decrease in the order of Fe, Co and Ni.

4. Numerical Simulations

As mentioned in the introduction, numerical simulations are carried out only for I-type spherules. We firstly investigate temperature dependence of equilibrium oxygen fugacity for Fe and Ni oxidation. For example, the equilibrium oxygen fugacity for the

Fe-Fe_3O_4 ($f_{O_2,T}$) system at temperature T is evaluated using

$$\log_e f_{O_2,T} = \frac{\frac{1}{2} G_{Fe_3O_4,T} - \frac{3}{2} G_{Fe,T} - G_{O_2,T}}{RT}, \quad (1)$$

where $G_{Fe_3O_4,T}$, $G_{Fe,T}$ and $G_{O_2,T}$ represent the standard free energies for formation of Fe_3O_4, Fe and O_2 at temperature T, respectively, and R is the gas constant. Thermochemical data are taken from BARIN *et al.* (1989) and SAXENA *et al.* (1993). Boundary curves between metals and their oxides of liquid phase are given in Fig. 5. Above the Ni-NiO boundary, Ni becomes Ni oxide (NiO), while below the boundary Ni is stable in the metal phase. The valence of Co is same as that of Ni, so Co is oxidized similarly to Ni. All Fe is oxidized as Fe^{3+} and incorporated into Fe_2O_3 above the Fe-Fe_2O_3 boundary. Between the Fe-Fe_2O_3 and Fe-FeO boundaries, Fe is oxidized as Fe^{2+} and Fe^{3+} to define the FeO-Fe_2O_3 boundary. On the Fe-Fe_3O_4 boundary, Fe^{2+}/Fe^{3+} ratio is 0.5 and additional Fe is oxidized with increasing $f_{O_2,T}$ to form stoichiometric Fe_3O_4. This diagram is, however, applicable to oxidation only in equilibrium and pure phases.

To predict the structure of I-type spherules by numerical simulations, it is important to identify that portion of the path on the f_{O_2} *vs* T diagram (Fig. 5) where spherules probably experienced heating during atmospheric entry. Therefore, numerical simula-

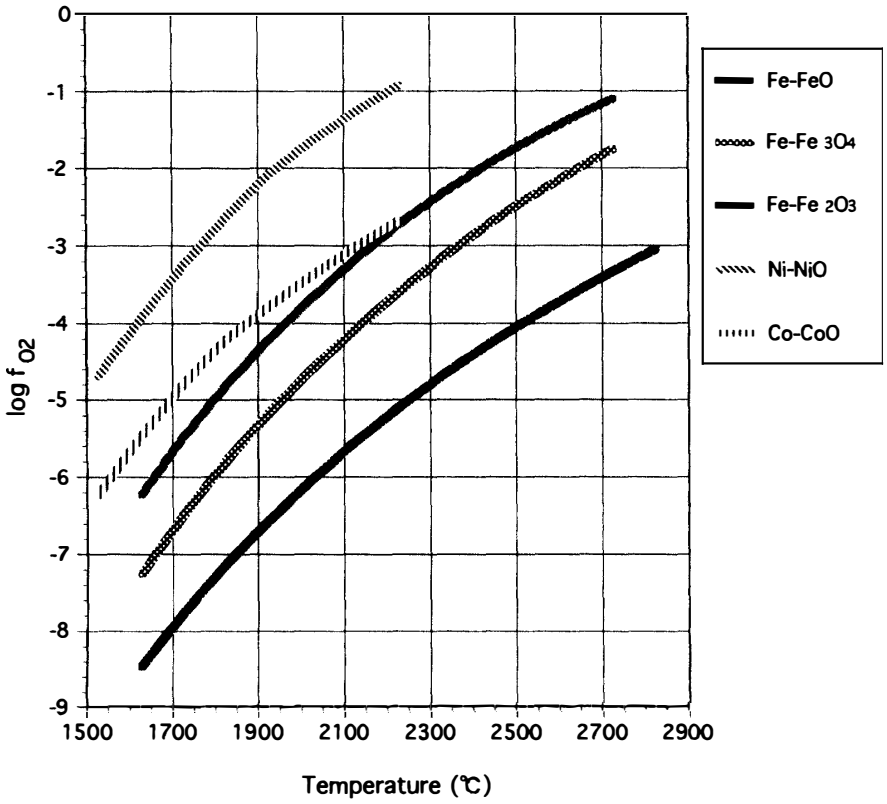

Fig. 5. Temperature dependence of log f_{O_2}. Above the boundary curves, the elements will be oxidized. Below the boundary, they will not be oxidized and will be stay in the metal phase. These boundary conditions are applicable only for pure phases in equilibrium.

tions were performed to model the atmospheric entry of the precursor spherule.

Starting at an altitude of 200 km, we simulate an iron sphere of initial radius r_0 coming into the earth's atmosphere with initial entry speed v_0 at an angle θ_0 from the local vertical at the starting altitude. The equation of energy conservation is

$$\pi r^2 \cdot \rho_{air} v \mathrm{d}t \cdot \frac{1}{2} v^2 \cdot \varepsilon_{th} - 4\pi r^2 \sigma T^4 \cdot \varepsilon_{em} \mathrm{d}t + L \cdot 4\pi r^2 \mathrm{d}r \cdot \rho_{mat} - \frac{4}{3}\pi r^3 \rho_{mat} C_P \mathrm{d}T + \Delta H_T \mathrm{d}m_{ox} = 0, \quad (2)$$

where r the radius of spherule, ρ_{air} the density of air at altitude where it exists, v the spherule's speed, ε_{th} the transform efficiency from the relative kinetic energy of the atmospheric molecules to the frictional heat, σ the Stefan-Boltzmann constant, T its temperature, ε_{em} the radiative efficiency, L the latent heat of evaporation of iron, ρ_{mat} the density of iron, C_P the specific heat capacity of iron at a constant pressure P, ΔH_T the heat of oxidation for iron and m_{ox} the moles of oxygen molecules consumed to oxidize iron. Value of ε_{th} and ε_{em} are assumed to be 1 here. The first term of left-hand side expresses the heating by the kinetic energy flux of atmospheric moledules colliding with the spherule. The second term denotes the radiative heat loss from the surface. The third term represents the heat lost by evaporation. The forth term is the heat capacity of the spherule. The last term depicts the heat of oxidation. Unfortunately, the oxidation rate of iron is difficult to determine. However, we can omit the last term in this numerical simulation because the heat of oxidation is estimated much less than the kinetic energy of atmospheric molecules cooliding wit the spherule (see Appendix). Since the forth term is also ascertained to be small, it is ignored.

If the sperule loses its mass only by evaporation, the equation of mass balance is written as follows:

$$4\pi r^2 \mathrm{d}r \cdot \rho_{mat} = -\frac{P(T)\sqrt{m}}{\sqrt{2\pi\kappa T}} \cdot 4\pi r^2 \mathrm{d}t, \quad (3)$$

where $P(T)$ is the saturated vapor pressure of iron at T, m the atomic mass of iron κ the Bolzmann constant. The left-hand term stands for the lost mass at dr. The right-hand term expresses the lost mass by using the saturated vapor pressure of iron.

The equation of momentum conservation is given by

$$\frac{4}{3}\pi r^3 \rho_{mat} \frac{\mathrm{d}\boldsymbol{V}}{\mathrm{d}t} = \frac{4}{3}\pi r^3 \rho_{mat} \boldsymbol{g} - \frac{1}{2} C_D \rho_{air} v \pi r^2 \boldsymbol{V} + 4\pi r^2 \rho_{mat} \boldsymbol{V}' \frac{\mathrm{d}r}{\mathrm{d}t}, \quad (4)$$

where $\boldsymbol{V}$ is the velocity of the sphere, $\boldsymbol{g}$ the gravitational acceleration vector and C_D the drag constant (C_D=2 in the supersonic condition (ADACHI *et al.*, 1976)), $\boldsymbol{V}'$ the mean relative velocity of evaporated iron atoms with respect to the spherule. Equation (4) shows that the derivative of a spherule's momentum with respect to time is balanced with the forces by terrestrial gravitation, atmospheric drag and the reaction of evaporation iron. We assume isotropic evaporation with respect to the spherule and put $\boldsymbol{V}'$=0.

The apparent gravitational acceleration in the frame of reference moving with the spherule is given by

$$g'=g-\frac{dV}{dt}, \tag{5}$$

This value is important for considering the formation of I-type spherules, which will be discussed later.

While the spherule travels through the atmosphere at a supersonic speed, the fugacity of O_2 it experiences is expressed by

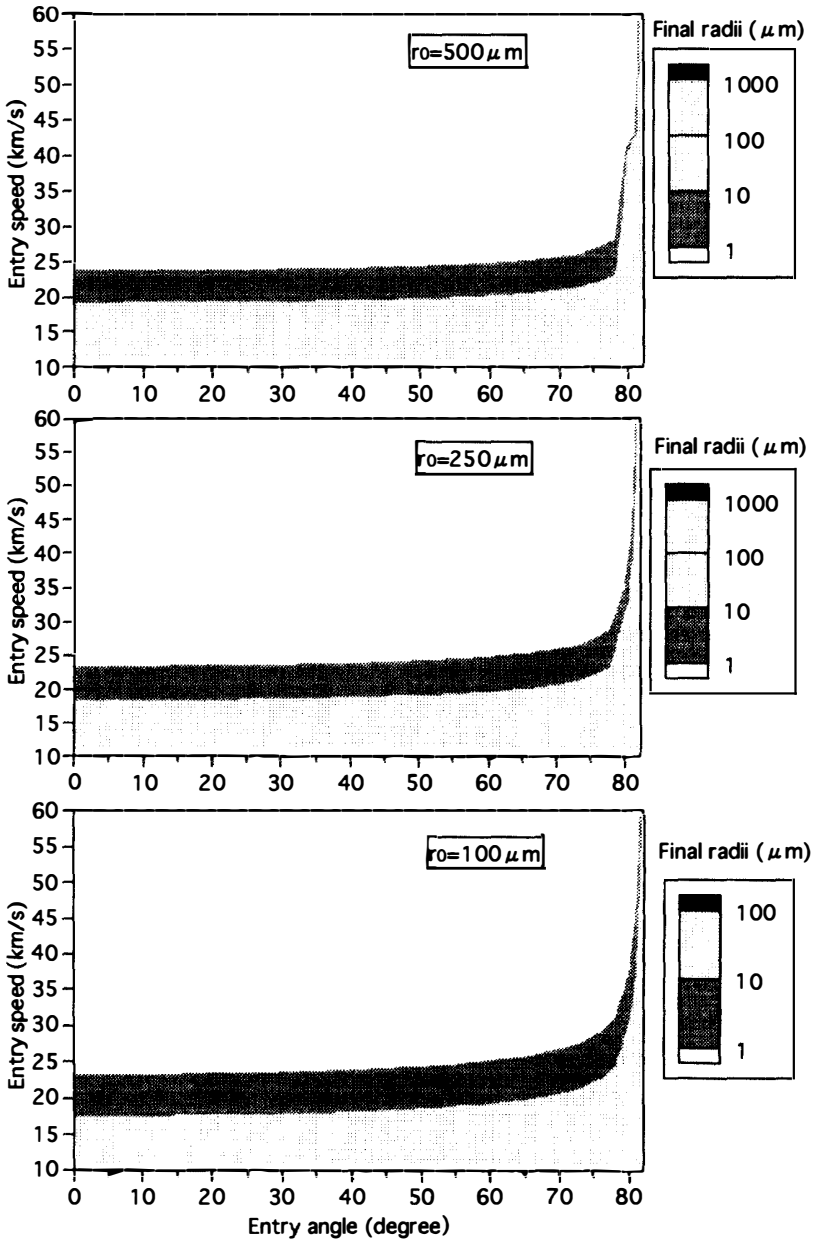

Fig. 6a. Final radii of spherules simulated for initial radii of 500 μm (upper), 250 μm (middle) and 100 μm (lower) with different entry angles and speeds. Over 25 km/s entry speed, spherules will perish except for high entry angles.

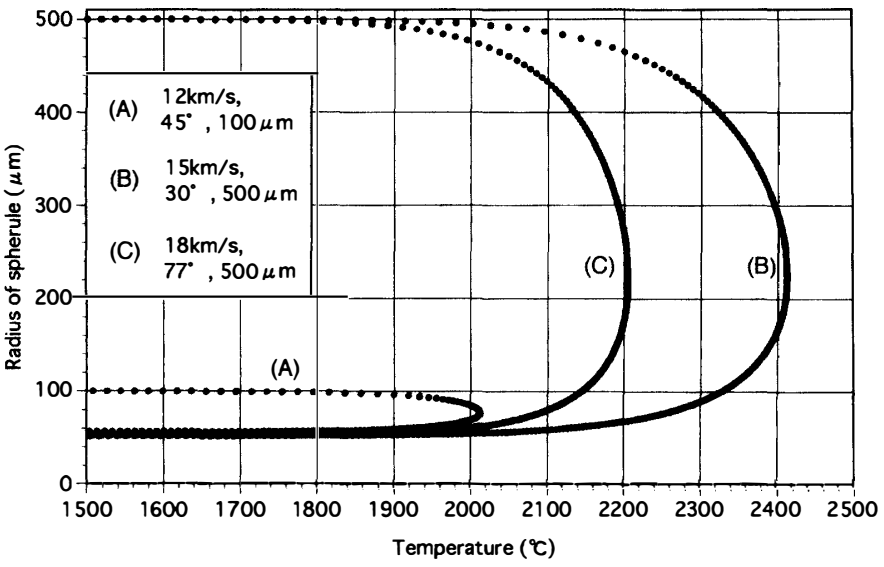

Fig. 6b. Temperature dependence of radii of spherules at three sets of initial conditions. Final radii are all approximately 50 μm. This graph shows the mass loss proceeds rapidly over 1900 °C.

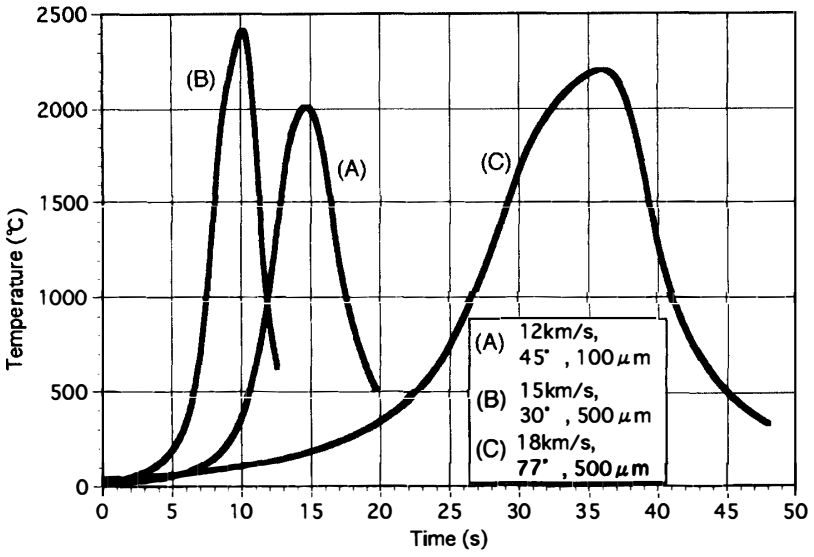

Fig. 6c. Time dependence of temperature of spherules with the same initial conditions as (b). This graph shows that the peak temperature increases as entry speed increases and that heating time increases as entry angle decreases.

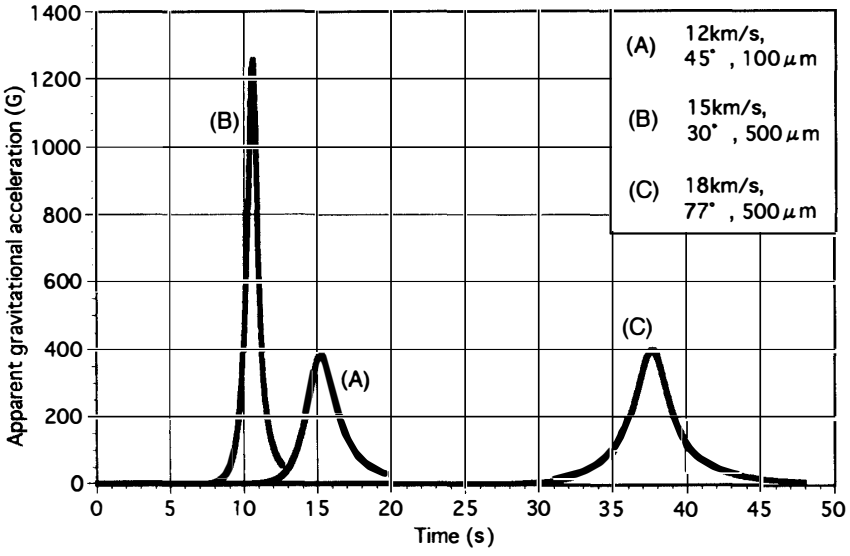

Fig. 6d. Time dependence of the apparent gravitational acceleration in the frame moving with a spherule. The acceleration is expressed in unit of the terrestrial surface gravitational acceleration, G. This graph shows that the apparent gravitational force on spherules increases as the entry speed increases and entry angle decreases.

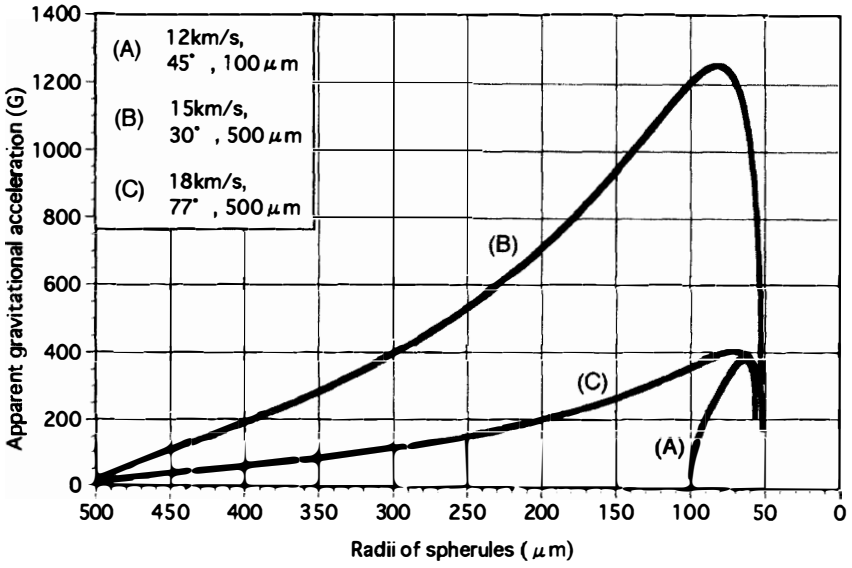

Fikg. 6e. Relation between radius of spherule and apparent gravitational acceleration. Gravitational acceleration is at a maximum value during the last stage of evaporation.

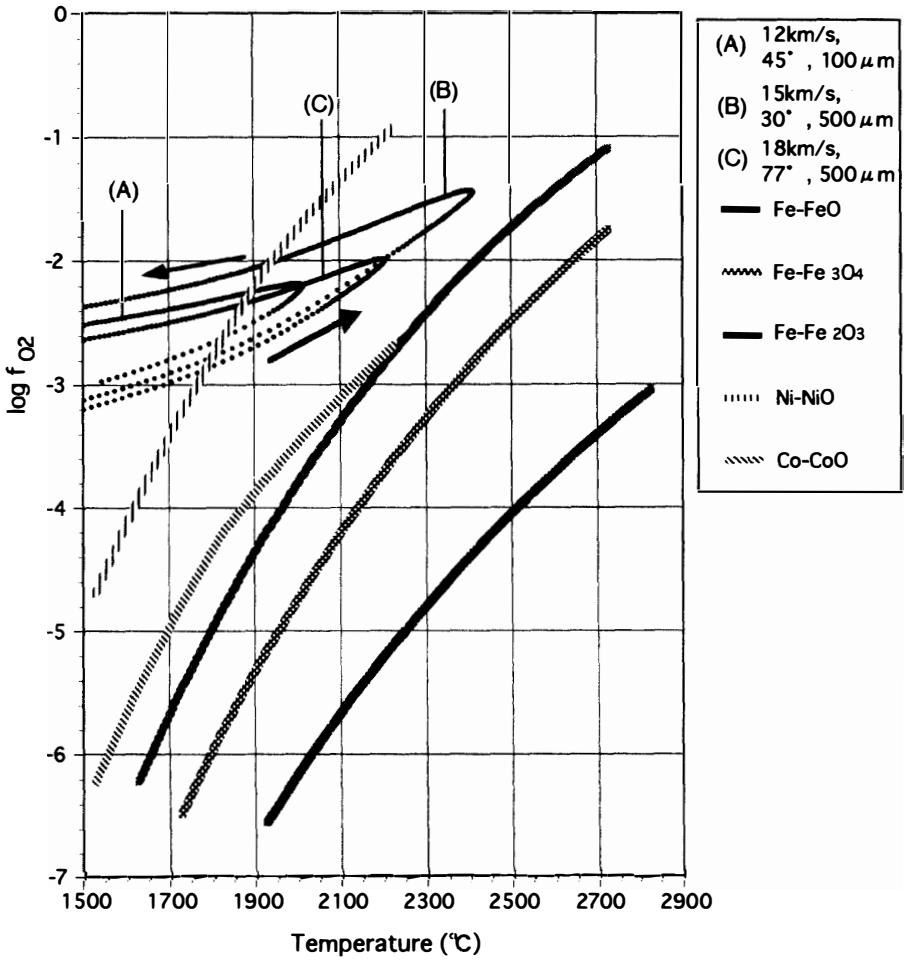

Fig. 6f. Oxygen fugacity f_{O_2} and temperature which spherules experience during atmospheric entry are plotted on the log f_{O_2}-T diagram (Fig. 5). Oxidation of spherules advances along arrows on the paths given in the diagram.

$$f_{O_2}=\frac{\rho_{air}v^2}{4\times10^6}, \tag{6}$$

where units of the right-hand term are in c.g.s. and f_{O_2} is the ratio of O_2 fugacity to that on the Earth surface. The right hand side of this equation expresses the dynamical pressure of oxygen. Note that static pressure is negligible in a highly supersonic situation. On the basis of eqs. (2)–(6), we calculate the time dependence of velocity, altitude, spherule's radius and temperature using the Runge-Kutta method. For data on air density at a given altitude, we use the U. S. Standard Atmosphere (1976). The vapor pressure and latent heat of iron are from KUBASCHEWSKI *et al.* (1967).

The radii of spherules obtained from various initial conditions are shown in Fig. 6a. With low angle (<75°) entry, meteoroids perish at any entry speeds over 25 km/s for this three initial radii. Special attention was given to cases where the final radii are about 50 μm, because these are representative of the observed sizes (Fig. 3d–f). Our calculations indicate that the spherule loses nearly 90 to 99.9% in this three types of initial conditions (Fig. 6b). The amount that spherules decrease in size depends on temperature, and is always most significant over 1900°C. The temperature that spherules experienced is shown in Fig. 6c. These demonstrate that the heating time is longer for the higher entry angle. During the heating and the ablation, micrometeoroids severely decelerate and experience a large apparent gravitational acceleration. Figure 6d shows the time dependence of apparent gravitational acceleration that results from the deceleration of spherules by atmospheric drag. Both high speed and low angle entry cause the large apparent gravitational acceleration. Figure 6e shows in what stage the apparent gravitational acceleration is strong. It is clear that the apparent gravitational acceleration is maximum at almost final stage of evaporation. In Fig. 6f, the oxygen fugacity f_{O_2} and the temperature of spherules during atmospheric entry are plotted on the $\log f_{O_2}$-T diagram (Fig. 5). The dependence of f_{O_2} on the initial conditions is minor, while the maximum temperature is dependent largely on initial conditions.

5. Discussion

Our cooling rate of the relict olivine grain can be compared with a previous simulation work for silicious micrometeoroids (LOVE and BROWNLEE, 1991). These authors calculated the cooling rates for silicious spherules of about 100 μm in final radii, which range from 44 to 500°C/s. Although the cooling rate by LOVE and BROWNLEE was calculated at various peak temperatures and cannot be compared directly with our work, we note that our cooling rate of the relict grain fits the lowest end of their cooling rates.

According to our numerical simulations, I-type spherules will lose their mass in a few seconds during the atmospheric entry, as reported by LOVE and BROWNLEE (1991). And the calculated mass loss of most of the spherules is consistent with that estimated from mass fractionations of Ni isotopes measured for I-type spherules, resulting from evaporation (HERZOG *et al.*, 1994).

Now we consider the oxidation effect on the internal structure of spherules based on the results of simulations. Spherules of over 50 μm in final radii usually lose most of the original mass and oxidation products which were formed before the intense evapora-

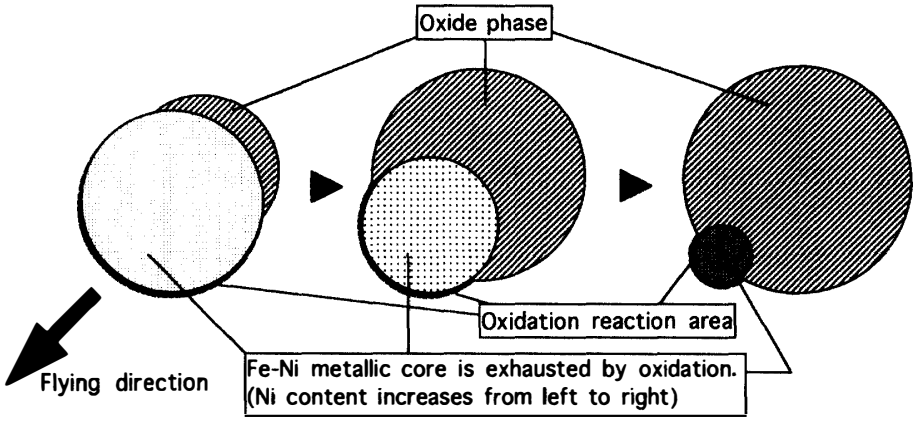

Fig. 7. A schematic diagram illustrating the oxidation process. During the oxidation of I-type spherules, off-centered metallic core material is exposed to the air due to the strong apparent gravitational acceleration. Oxidation reactions produce an oxide mantle where the metallic core is exposed at the surface of the spherule.

tion. Consequently, the early oxide products should be eliminated from the spherules. The oxide phase that composed I-type spherules is assumed to be formed between the end of evaporation and the solidification. Hence, we emphasize the oxidation process at this stage. As shown in Figs. 6d and e, the apparent gravitational acceleration reaches maximum and then gradually decreases. Iron oxides envelop a Fe-Ni metallic core because metal has a larger surface tension than oxides. In a metallurgical experiment using a levitated apparatus with terrestrial gravity, Fe-oxide melt is distributed on one side of a iron metal sphere, and the oxidation of Fe proceeds on the metal surface exposed to the external gas (SUN and PEHLKE, 1994). For the case of cosmic spherules entering the atmosphere, the apparent gravitational acceleration acting on the spherules is much larger than the terrestrial one and some part of the surface of metallic core might always be exposed to the air. As a result, oxidation reaction would proceed on these surfaces, as shown in Fig. 7. The oxidation reaction rate at the liquid metallic surface from the atmosphere is much faster than that at the boundary of liquid metal and oxides. The oxidation of cosmic spherules ceases in a relatively short time span because the gravitational acceleration is weakened, causing the metallic core to be enveloped by the oxide layer.

Oxidation would not necessarily proceed along the paths as shown in diagram of Fig. 6g. In the oxidation process, Ni atoms in Fe are also oxidized when they impact with oxygen molecules. However, the NiO can be reduced by Fe atoms while it is moving to the oxide layer because Fe is easier to be oxidized. Therefore, only Fe might be oxidized to form a Ni-enriched metal core and an Fe oxide envelope that is free of Ni like Fig. 3d during the early stage of oxidation. On the surface of the metallic core where oxidation occurred, Ni atoms would begin to be oxidized. An oxide envelope containing NiO would be formed when Fe atoms on the surface are completely oxidized and removed from the oxide envelope. Thus, the Ni atoms remain. When the oxidation stops and the system becomes equilibrium before its solidification, NiO will be completely reduced. In contrast, when the solidification occurs at disequilibrium, NiO are

left in the oxide envelope and a spherule with a Fe-Ni metallic core and a Fe-Ni oxide mantle will be formed (possibly, Fig. 3f).

Sometimes metal cores escape from oxide envelopes, as BI *et al.* (1993) observed. We suggest that Fe and Ni are completely oxidized, as in Fig. 3f, when the apparent gravitational acceleration can't overcome the surface tension of Fe oxide, causing the metallic core to be continuously oxidized at the exposed surface of the spherule until it perishes. This model explains the off-centered distribution of many spherule cores.

6. Conclusions

(1) The following S-type spherules are distinguished: porphyritic type, barred type and fine-grained type. A cooling rate of a relict grain contained in one of the S-type spherules is calculated to be 55°C/s from profile fitting with a peak temperature of 1700°C.

(2) Two types of I-type spherules including Ni are distinguished: spherules with Fe oxide mantles and Fe-Ni metallic cores and Fe-Ni oxide spherules without metallic cores. Some spherules with a Fe-Ni oxide mantle and a Fe-Ni metallic core may also exist.

(3) Result of our numerical simulation indicate that I-type spherules lose most of their original mass during their atmospheric entry. The mass loss of spherules occurs over about 1900°C and the apparent gravitational acceleration acting on them become maximum at the last stage of mass loss. Depending on the acceleration experienced, metallic cores of the spherules are exposed to the air and oxidized, off-centered, or ejected entirely from the spherule.

Acknowledgments

We are grateful to late Prof. K. YAMAKOSHI, Institute of Cosmic Ray Research, University of Tokyo, for providing samples of deep sea sediments. We thank specially Prof. M. MIYAMOTO for calculation of the cooling rate of relict grains. Our thanks go to Prof. H. CHIBA and Prof. K. NAKAJIMA for advising us about the temperature-logf_{O_2} diagram , and Dr. H. SUN for discussing about the oxidation process of spherules. Prof. G.J. FLYNN, Dr. Y. TAZAWA, and Dr. L.B. BROWNING gave us constructive and useful comments which helped improve the manuscript.

References

ADACHI, I., HAYASHI, C. and NAKAZAWA, K. (1976): The gas drag effect on the elliptic motion of a solid body in the primordial solar nebula. Prog. Theor. Phys., **56**, 1756–1771.

BARIN, I., SAUERT, F., SCHULTZE-RHONHOF, E. and SHENG, W.S. (1989): Thermochemical Data of Pure Substances. Weinheim, VCH Pub., 1739p.

BI, D., MORTON, R.D. and WANG, K. (1993): Cosmic nickel-iron alloy spherules from Pleistocene sediments, Alberta, Canada. Geochim. Cosmochim. Acta, **57**, 4129–4136.

BLANCHARD, M.B., BROWNLEE, D.E., BUNCH, T.E., HODGE, P.W. and KYTE, F.T. (1980): Meteoroid ablation spheres from deep-sea sediments. Earth Planet. Sci. Lett., **46**, 178–190.

BROWNLEE, D.E. (1985): Cosmic dust: Collection and research. Ann. Rev. Earth Planet. Sci., **13**, 147–173.

BROWNLEE, D.E., BATES, B.A. and WHEELOCK, M.M. (1984): Extraterrestrial platinum group nuggets in deep-

sea sediments. Nature, **309**, 693–695.
CLAYTON, R.N., MAYEDA, T.K. and BROWNLEE, D.E. (1986): Oxygen isotopes in deep-sea spherules. Earth Planet. Sci. Lett., **79**, 235–240.
CZAJKOWSKI, J. (1987): Cosmo and geochemistry of the Jurassic hardgrounds. Ph. D. diss., Univ. California, San Diego.
HERZOG, G.F., HALL, G.S. And BROWNLEE, D.E. (1994): Mass fractionation of nickel isotopes in metallic cosmic spheres. Geochim. Cosmochim. Acta, **58**, 5319–5323.
KUBASCHEWSKI, O., EVANS, E. Ll. and ALCOCK, C. B. (1967): Metallurgical Thermochemistry, 4th ed. Oxford, Pergamon Press, 495p.
LOVE, S.G. and BROWNLEE, D.E. (1991): Heating and thermal transformation of micrometeoroids entering the Earth's Atmosphere. Icarus, **89**, 26–43.
MARVIN, U.B. and EINAUDI, M.T. (1967): Black, magnetic spherules from Pleistocene and recent beach sands. Geochim. Cosmochim. Acta, **31**, 1871–1884.
MILLARD, H.T., Jr. and FINKELMAN, R.B. (1970): Chemical and mineralogical compositions of cosmic and terrestrial spherules from a marine sediment. J. Geophys. Res., **75**, 2125–2134.
MIYAMOTO, M., MCKAY, D. S., MCKAY, G. A. and DUKE, M. B. (1986): Chemical zoning and homogenization of olivines in ordinary chondrites and implications for thermal histories of chondrules. J. Geophys. Res., **91**, 12804–12816.
MURRAY, J. and RENARD, A.F. (1883): On the measurement characters of volcanic ashes and cosmic dust, and their origin in deep-sea sediment deposits. Proc. R. Soc. Edinburgh, **12**, 474–495.
NISHIIZUMI, K. (1983): Measurement of ^{53}Mn in deep-sea iron and stony spherules. Earth Planet. Sci. Lett., **63**, 223–228.
RAISBECK, G. M., YIOU, F., BOURLES, D. and MAURETTE, M. (1986): ^{10}Be and ^{26}Al in Greenland cosmic spherules; evidence for irradiation in space as small objects and a probable cometary origin. Meteoritics, **21**, 487–488.
SAXENA, S.K., CHATTERJEE, N., FEI, Y. and SHEN, G. (1993): Thermodynamic Data on Oxides and Silicates. Berlin, Springer, 428p.
SMALES, A.A., MAPPER, D. and WOOD, A. J. (1958): Radioactivation analysis of "cosmic" and other magnetic spherules. Geochim. Cosmochim. Acta, **13**, 123–126.
SUN, H. and PEHLKE, R. D. (1994): Modeling and experimental study of gaseous oxidation of liquid iron alloys. submitted to Metall. Mat. Trans. B.
U. S. Standard Atmosphere (1976): U. S. Gonvt. Printing Office, Washington, D.C., 227p.

(Received September 25, 1995; Revised manuscript accepted November 29, 1995)

Appendix

To confirm the influence of the heat of oxidation on the simulation, we compare the contribution of heat of oxidation with kinetic energy due to atmospheric molecules' collision. The heat of oxidation is equal to the difference of enthalpy (ΔH_T) between the source and the product, calculated by

$$\Delta H_T = 2H_{T,\mathrm{Fe}} + H_{T,\mathrm{O_2}} - 2H_{T,\mathrm{FeO}}, \tag{A1}$$

where $H_{T,\mathrm{Fe}}$, $H_{T,\mathrm{O_2}}$ and $H_{T,\mathrm{FeO}}$ represent the enthalpy of Fe, O_2 and FeO at temperature T. In a solid phase, the oxidation rate is much slower than that in a liquid phase and is controlled by mutual diffusion speed of oxygen and iron ions in an oxide layer, because the oxide layer is formed on the spherules' surface. So spherules are mainly oxidized at liquid phase. ΔH_T ranges from 5.13 to 5.05×10^{12} erg/mol at temperature between 1800 to 3000 K. We assume 5.1×10^{12} erg/mol for ΔH_T at any temperature. Thermochemical

data are cited from BARIN *et al.* (1989).

The simulation is based on the assumption that every O_2 molecules that hits on the spherule is used to oxidize metallic iron. Thus, the estimated heat of oxidation is a maximum value of that we can estimate. Initial conditions are set to r_0=100 μm, v_0=12 km/s, and θ_0=45°. The velocity of 12 km/s is roughly a minimum value for the entry velocity for meteoroids, so the kinetic energy flux of atmospheric molecules colliding with the spherule is also roughly at a minimum. The result of calculation is shown in Fig. A1. The heat of oxidation is about one twentieth of the kinetic energy flux of atmospheric molecules colliding with the spherule. Moreover, there is little difference between the case including the heat of oxidation and that omitting it: 15°C in peak temperature and 7 μm in final radius. For the case of lower angle and/or larger velocity entry, the influence of oxidation heat on the simulation is significantly lessened.

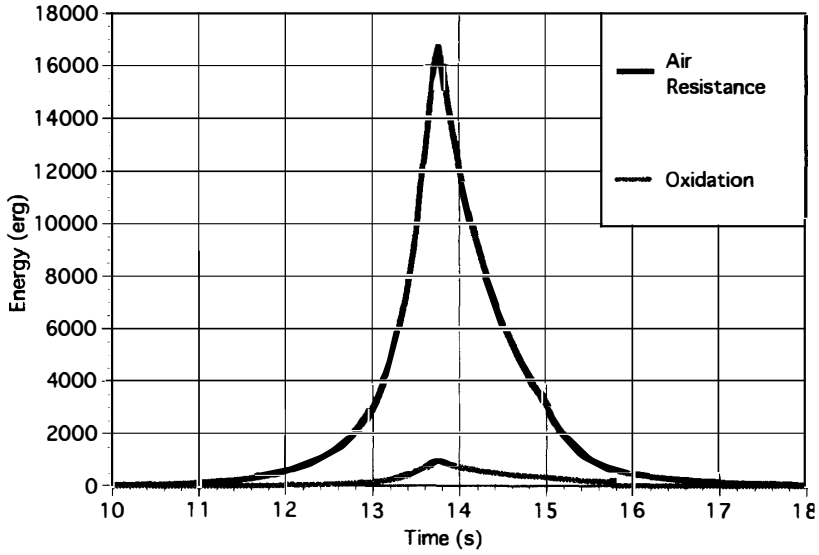

Fig. A1. The time dependence of the reaction energy of oxidation and the kinetic energy flux of atmospheric molecules colliding with the spherule. The initial conditions are: 100 mm for r_0, 12 km/s for v_0 and 45° for q_0. The heat of oxidation is about one twentieth of kinetic energy flux of atmospheric molecules colliding with the spherule.